The ultrastructure of the *Chlamydomonas reinhardtii* basal apparatus: identification of an early marker of radial asymmetry inherent in the basal body

Stefan Geimer* and Michael Melkonian

Botanisches Institut, Universität zu Köln, Gyrhofstr. 15, 50931 Köln, Germany

*Author for correspondence (e-mail: stefan.geimer@uni-koeln.de)

Accepted 23 January 2004
Journal of Cell Science 117, 2663-2674 Published by The Company of Biologists 2004
doi:10.1242/jcs.01120

Summary

The biflagellate unicellular green alga *Chlamydomonas reinhardtii* is a classic model organism for the analysis of flagella and their organizers, the basal bodies. In this cell, the two flagella-bearing basal bodies, along with two probasal bodies and an array of fibers and microtubules, form a complex organelle called the basal apparatus. The ultrastructure of the basal apparatus was analysed in detail by serial thin-section electron microscopy of isolated cytoskeletons and several newly discovered features are described, including a marker for the rotational asymmetry inherent in the basal bodies and probasal bodies. In addition, the complex three-dimensional basal apparatus ultrastructure is resolved and illustrated, including the attachment sites of all basal apparatus elements to specific microtubular triplets of the basal bodies and probasal bodies. These data will facilitate both the localization of novel basal apparatus proteins and the analysis of mutants and RNA interference cells with only subtle defects in basal apparatus ultrastructure. The early harbinger of radial asymmetry described here could play a crucial role during basal body maturation by orienting the asymmetric attachment of the various associated fibers and therefore might define the orientation of the basal bodies and, ultimately, the direction of flagellar beating.

Key words: Basal apparatus, Basal body, *Chlamydomonas reinhardtii*, Flagellate green alga, Probasal body, Rotational asymmetry

Introduction

Basal bodies (present at the base of cilia and flagella) and centrioles (which form the core of the centrosome in mammalian cells) are two manifestations of the same conserved eukaryotic organelle. They consist of nine triplets of microtubules arranged in a ninefold radially symmetric array. Basal bodies and centrioles display structural and functional polarities that play an important role in the spatial arrangement of the cytoskeleton and hence the polarity of the cell and, in the case of basal bodies, the direction of ciliary/flagellar beat (reviewed in Beisson and Jerka-Dziadosz, 1999; Preble et al., 2000).

The basal apparatus of the biflagellate green alga *Chlamydomonas reinhardtii* is a complex organelle located at the anterior end of the cell consisting of two basal bodies (often referred to as mature basal bodies), two probasal bodies (nascent basal bodies) and an array of fibers and microtubules appended to each basal body in an asymmetric manner. The basal bodies are anchored to the cell membrane, organize the formation of the flagella and serve as an organizing center for the microtubular cytoskeleton in interphase and mitosis (reviewed in Dutcher, 2003).

Green flagellates are excellent model organisms for the analysis of the function and protein composition of basal bodies (reviewed in Marshall and Rosenbaum, 2000). The ubiquitous centrosomal protein centrin (also known as caltractin) was first discovered as the major component of a basal-body-associated fiber in a green alga (reviewed in Salisbury, 1995). The biochemical analysis of isolated basal apparatuses from the green flagellate *Spermatozopsis similis* led to the identification of several novel basal apparatus proteins (SF-assemblin, BAp95, BAp90 and p210) that are localized to different fibers associated with specific sites of the basal bodies (Lechtreck and Melkonian, 1991; Geimer et al., 1998a; Geimer et al., 1998b; Lechtreck et al., 1999). In *Chlamydomonas*, mutations affecting basal body function can be identified by the absence of flagella or their presence in an aberrant number (*bld* mutants are bald, having no flagella; *uni* mutants are uniflagellate; *vfl* mutants have a variable number of flagella). The *UNI3* gene has been shown to encode an entirely new class of tubulin, δ-tubulin (Dutcher and Trabuco, 1998), and the Vfl1 and Vfl3 proteins are thought to play a role in the rotational orientation of the basal bodies (Silflow et al., 2001; Silflow and Iyadurai, 2002). Within the past few years, new molecular tools have been established, such as *Chlamydomonas*-adapted green fluorescent protein (GFP) (Fuhrmann et al., 1999) and RNA interference methods (Fuhrmann et al., 2001), which can be used for the in vivo analysis of basal apparatus proteins (Ruiz-Binder et al., 2002; Lechtreck et al., 2002; Koblenz et al., 2003). These tools, together with the availability of large expressed sequence tag databases (Asamizu et al., 1999; Asamizu et al., 2000; Shrager et al., 2003), the complete nuclear genome sequence (http://www.biology.duke.edu/chlamy_genome/cgp.html) and

progress in proteome research will greatly facilitate the molecular analysis of the basal apparatus.

The overall structure of the *Chlamydomonas* flagellar apparatus (the flagella and the basal apparatus) and the major ultrastructural components of the basal apparatus have been described in two classic studies (Ringo, 1967; Cavalier-Smith, 1974), but these data are not sufficiently detailed for the new tasks. This is illustrated by a recent study in which minor defects in the basal bodies of a *Chlamydomonas* δ-tubulin deletion mutant were detected using dual-axis electron tomography (O'Toole et al., 2003). We felt that a detailed high-resolution map integrating all structural components of the *Chlamydomonas* basal apparatus was needed and decided to reinvestigate its ultrastructure using serial ultrathin sections of isolated cytoskeletons. We describe several novel aspects of the basal apparatus architecture (including new information about the attachment of the microtubular flagellar roots to specific basal body triplets), a numbering system for the triplets of the probasal bodies and a detailed diagram illustrating how all components of the basal apparatus together form the highly ordered architecture of this complex proteinaceous machinery. Most importantly, a structural marker for the rotational asymmetry inherent in the basal bodies and probasal bodies has been discovered. This structure (termed the 'acorn') is attached to the inner wall of the microtubular cylinder at its distal end, representing the counterpart of the well known cartwheel usually present at the proximal end of basal bodies and centrioles. Whereas the cartwheel is thought to nucleate the ninefold rotational symmetry of the microtubular triplets (reviewed in Beisson and Wright, 2003), the acorn might play an equally important role imposing rotational asymmetry on the microtubular triplets, perhaps leading to the asymmetric assembly of basal-body-associated fibers and hence cellular asymmetry in general.

Materials and Methods

Strains and culture conditions

C. reinhardtii cw 15^+ Dangeard (SAG 83.81) (Schlösser, 1994) was cultured in aerated 10 l flasks (~1 l $minute^{-1}$) at 15°C with a light:dark cycle of 14:10 hours and a photon flux density of 20 μE m^{-2} $second^{-1}$ (Osram 40W/25 universal white) in WarisH culture medium (McFadden and Melkonian, 1986).

Isolation of cytoskeletons

Cytoskeletons were isolated as described in Wright et al. (Wright et al., 1985).

Fixation and embedding for standard electron microscopy

The isolated cytoskeletons were resuspended in MT buffer (30 mM HEPES, 5 mM Na-EGTA, 15 mM KCl, pH 7.0), fixed by adding an equal volume of 5% glutaraldehyde in MT buffer for 15 minutes at 15°C, sedimented (1000 ***g*** for 10 minutes) and resuspended in MT buffer containing 1.25% glutaraldehyde and 0.5% tannic acid (TAAB, Aldermaston, UK). After 25 minutes at 15°C, the cytoskeletons were sedimented, washed twice in MT buffer and osmicated for 20 minutes (1% OsO_4 in MT buffer) on ice. Pellets were washed twice in MT buffer, transferred to agar, dehydrated and embedded in Epon 812 (Serva, Heidelberg, Germany) as described by McFadden and Melkonian (McFadden and Melkonian, 1986).

Ultrathin sections and electron microscopy

Ultrathin serial sections (50-70 nm) were cut with a diamond knife (Delaware Diamond Knives, Wilmington, DE, USA) on a RMC MT 6000-XL microtome (RMC, Tucson, AZ, USA) and mounted on Pioloform-coated copper grids (Plano, Wetzlar, Germany). The sections were stained with lead citrate and uranyl acetate (Reynolds, 1963). Micrographs were taken with a Philips CM10 transmission electron microscope using Scientia EM Film (Agfa, Leverkusen, Germany). In cross-sectioned basal bodies or axonemes, the view is from the distal to the proximal end.

Results

Terminology and triplet numbering

For a general terminology of the components of the flagellar apparatus, see Andersen et al. (Andersen et al., 1991). All structures associated with the basal bodies (bbs), including the X-shaped 4-2-4-2 microtubular flagellar root system, were labeled as previously described, so 1 indicates an association with the older bb and 2 an association with the younger bb (Heimann et al., 1989; Moestrup and Hori, 1989), and s indicates sinister (left) and d dexter (right) of the bb viewed from its distal end with triplet 1 in the 12 o'clock position (Melkonian, 1984) (see Fig. 7G-I). The numbering of individual flagellar root microtubules follows Melkonian (Melkonian, 1978) (see Fig. 7G).

A numbering system of the bb triplets can be established by tracing axonemal doublets in serial sections from the axoneme down into the bb. In the axoneme of *Chlamydomonas*, doublet 1 is recognized by the absence of the outer dynein arm and a (two-part) bridge extending from its A-tubule to the B-tubule of doublet 2 (Fig. 1A,B, arrowheads) (Hoops and Witman, 1983). Triplet 1 of the bb is the middle of the three triplets to which the distal connecting fiber (dcf) is attached (Fig. 1A-J, arrowheads) (Hoops and Witman, 1983). A numbering system for the triplets of the probasal body (pbb) was established in this study (see below).

The acorn

At the distal end of the bb, exactly at the transition between the microtubular triplets of the bb and the doublets of the transitional region, a filament of about 10 nm diameter is attached to the microtubular doublets (rarely triplets) in a rotationally asymmetric pattern linking A-tubules of doublets 7, 8, 9, 1 and 2 (Fig. 1G, Fig. 2D,E). From doublet 2, the filament arches back to doublet 7, passing through the lumen of the bb. The overall outline of this closed structure resembles that of an (capless) acorn with its broad base located between doublets 1 and 2, and its pointed tip at doublet 7 (see schematic drawing Fig. 7D). At doublets 2 and 7, the acorn has a prominent knob through which linkage with the A-tubule is established. The side of the acorn that is not attached to bb doublets/triplets will, in the following, be called the 'lumenal' side of the acorn.

A second, V-shaped, system of filaments of about 8 nm diameter is present in this region of the bb. Two filaments extend from triplets (rarely doublets) 4 and 5 into the bb lumen, bisect the lumenal side of the acorn (Fig. 1G, Fig. 2D,E) and, in the center of the bb lumen, connect to another filament that runs perpendicular to the two filaments, extending down from

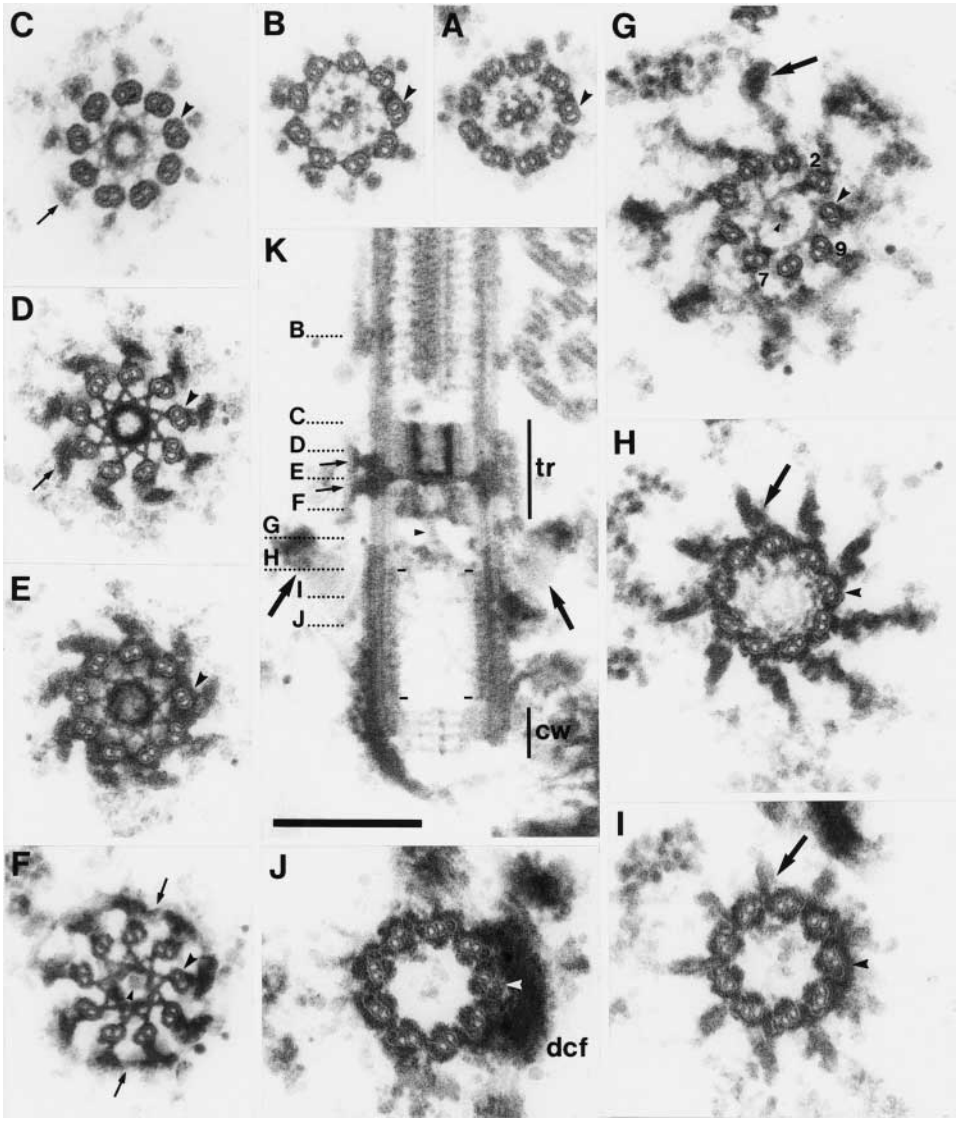

Fig. 1. The axoneme, transitional region and basal body. (A-J) Series of transverse sections (section numbers 1, 10, 13-20) showing the axoneme (A,B), transitional region with the distal stellate structure (C,D), transitional plate (E) and proximal stellate structure (F), and distal part of the bb (G-J). Within the axoneme, doublet 1 (A,B, arrowhead) can be identified by a bridge extending from its A-tubule to the B-tubule of doublet 2. This doublet (doublet/triplet 1 is marked with an arrowhead in C-J) is continuous with the middle of the three triplets to which the distal connecting fiber (dcf; J) is attached (J, arrowhead). In the transitional region, short, T-shaped fibers (the doublet outer projections; C,D,F,K, small arrows) are attached to the A/B-tubule junction on the outside of the doublets. In the area of the proximal stellate structure, the doublet outer projections are sometimes interconnected, forming a ring (F, small arrows). In the region of the transitional plate, the lumen of the transitional region is filled with electron-dense material that extends between the microtubular doublets into the doublet outer projections, which, at this level, form saw-tooth-like structures projecting from the microtubular cylinder (E). The transitional fibers (G-I,K, large arrows) are attached to the distal half of the bb. Within the microtubular cylinder – exactly at the transition between the microtubular doublets of the transitional region and the microtubular triplets of the bb – filaments are attached in a rotationally asymmetric pattern to the microtubular doublets/triplets (G) (Fig. 2D,E). A filament outlining the shape of an acorn is attached to the A-tubules of doublets 7, 8, 9, 1 and 2 (G, doublets 7, 9 and 2 are numbered). The lumenal side of the acorn is crossed by a V-shaped filament system; two filaments extend from triplets 4 and 5, and, in the center of the bb lumen, connect to another filament that runs perpendicular to the two filaments, extending down from the proximal end of the stellate structure in the transitional region (F,G,K, small arrowheads). The acorn and V-shaped filament system are already present at the distal end of the pbbs (Fig. 2A). (K) Median longitudinal section through the axoneme and bb showing the transitional region (vertical line labeled tr) and doublet outer projections (small arrows), the transitional fibers (large arrows), and the cartwheel (vertical line labeled cw). Sectional planes corresponding to transverse sections B-J are marked by dotted lines. Two rows of projections can be seen attached to the triplets and extending into the lumen of the bb (between two pairs of dashes). A fine filament (small arrowhead) interconnects the proximal end of the proximal stellate structure with the system of filaments present in the distal lumen of the bb (compare with F and G, showing this filament in transverse section, small arrowheads). Scale bar, 250 nm.

the proximal end of the stellate structure in the transitional region (Fig. 1G,K, small arrowheads). The positional relationships of the acorn to these filaments is best seen in longitudinal sections through bbs (Fig. 2G). In such sections, the acorn is seen as two asymmetrically positioned electron-dense dots (Fig. 2G, arrowheads). The filaments extend from triplets 4 and 5 at the level of the acorn and bend downwards with an angle of about 35° after reaching the lumenal side of the acorn. They continue to the other side of the bb, making contact with triplets at the level of the dcf attachment with the bb (Fig. 2G, small arrows). In cross sections through bbs, depending on the sectional plane, these filaments can be seen to contact triplets 8, 9 and 1 (Fig. 2E, arrowhead) (S. Geimer and M. Melkonian, unpublished).

Most interestingly, both systems of filaments were already present at the distal end of the probasal bodies (cross section in Fig. 2A, compare with Fig. 2D,E in the bb; longitudinal section in Fig. 2F, compare with Fig. 2G in the bb).

Basal bodies

The flagella-bearing bbs are composed of nine microtubular

triplets with connections between the A- and C-tubules of adjacent triplets (Fig. 3F). They have an average length of 320 nm (n=10) based on the length of the microtubular triplets and their diameter is about 210 nm (n=10). Most of the C-tubules in the bb triplets are filled with electron-dense material (Fig. 1H-J, Fig. 3F, Fig. 4A-E). At the proximal end of each bb, the hub and spoke complex of the cartwheel is present (Fig. 1K, cw; Fig. 3F) (Ringo, 1967). The cartwheel consists of a central hub (diameter about 25 nm, with a central dot; Fig. 3F, Fig. 4E) and nine spokes that are connected to the A-tubules by nine triangular electron-dense knobs (Fig. 3F, Fig. 4E) (Cavalier-Smith, 1974; O'Toole et al., 2003). The dot in the central hub might represent a fine filament in cross section because, in some median longitudinal sections of bbs, a fine filament was seen emanating from the central hub at the proximal end of the cartwheel (not shown).

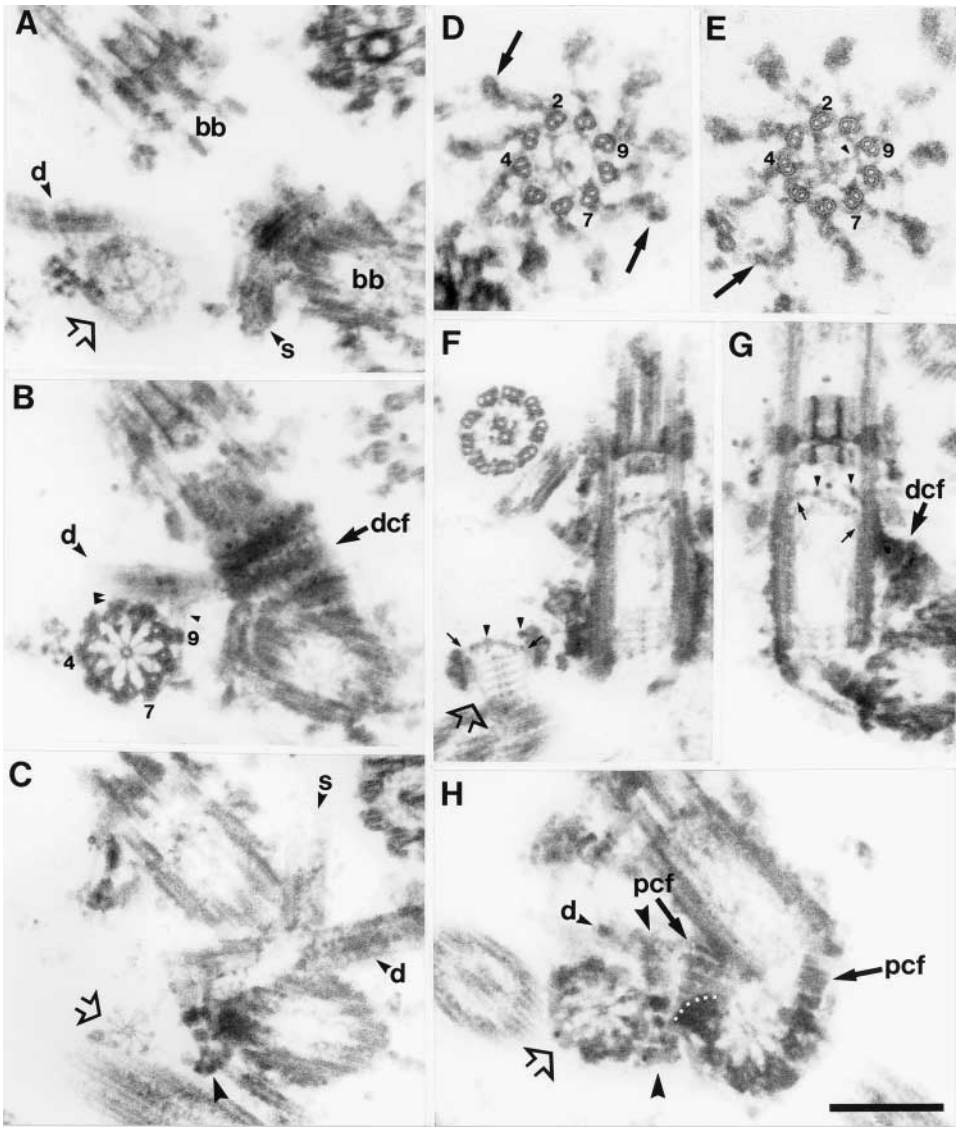

Fig. 2. The probasal body. (A-C) Consecutive transverse sections through a pbb; the two bbs are sectioned at an oblique angle. The microtubular roots (A-C, d for d-roots, s for s-roots) and the distal connecting fiber (B, dcf) are visible. At the distal end of the pbb (A, open arrow), the acorn and V-shaped filament system, which are also present at the distal end of the bb, can be seen (compare to bbs shown D and E; see also Fig. 1G). More proximally (B, pbb triplets are numbered), the microtubular triplets and the hub and spoke complex of the cartwheel are visible. The B- and C-tubules are filled with electron-dense material. An electron-dense patch is overlying the C-tubule of triplet 9 and filaments of the lateral striated fiber link at least triplets 7, 8 and 9 to the corresponding d-root (B, small arrowhead; see also Fig. 6E,F). Triplets 1 and 2 lie close to the d-root and corresponding striated microtubule-associated fiber (SMAF), and are connected to the SMAF by fine filaments (B, double arrowhead; see also Fig. 6H). At the most proximal end of the pbb, only the hub and spoke complex of the cartwheel, protruding from the microtubular cylinder, is visible (C, compare with longitudinal sectioned pbb in F, open arrows). The lateral striated fiber is labeled (C, large arrowhead). (D,E) Transverse sections through the most distal end of bbs showing the acorn and V-shaped filament system (triplet numbers are indicated, compare with Fig. 1G). The transitional fibers are marked (large arrows). In E, the two filaments that extend from triplets 4 and 5, and fuse in the center of the bb, continue and make contact with doublet 9 (small arrowhead). (F) Longitudinal section through a bb and pbb (open arrow). The cartwheel of the pbb consists of six tiers, of which only three are bound by the short microtubular triplets. Also, in longitudinal section, the filamentous system present at the distal end of the pbb clearly resembles that present within the lumen at the distal end of the bb. This becomes clear from a comparison of the pbb shown in F with the bb shown in G. The acorn is seen as two asymmetrically positioned electron-dense dots in the bb (Fig. 2G, small arrowheads) and pbb (Fig. 2F, small arrowheads). The filaments extending from triplets 4 and 5 at the level of the acorn (small arrow at the left side of the pbb in F and bb in G) bend downwards with an angle of about 35° (referring to the transverse axis of the pbb/bb) after reaching the lumenal side of the acorn and continue to the other side of the pbb/bb. In the pbb, these filaments make contact with triplets and the cartwheel (F, small arrow at the right side of the pbb). In the bb, these filaments make contact with triplets at the level of the dcf attachment with the bb (G, small arrow at the right side of the bb). (H) Section through a basal apparatus; one bb is sectioned longitudinally, the other one transversely. The proximal connecting fibers interconnecting the bbs are visible (pcf). The transversely sectioned pbb (open arrow) is attached by the lateral striated fiber (see also C, large arrowheads) to the corresponding d-root (d). The lateral striated fiber also interconnects the pbb with parts of the sf^2 and probably the pcf. The limits of the sf^2 to the pcf are outlined by white squares. Scale bar, 250 nm.

In the present study, the developmental status of the bbs was deduced based on the number of cartwheel tiers. It has been shown previously in other flagellate green algae that the cartwheel of the developmentally oldest bb (bb 1) shows fewer tiers than the cartwheel of the younger bb(s) (Beech et al., 1991; Beech and Melkonian, 1993). Because serial sectioning through both bbs (n=10) consistently revealed that there are differences in the number of cartwheel tiers in the two bbs we assume that the same is true for *C. reinhardtii* and thus label as 1 the bb that has the fewer cartwheel tiers (Fig. 3A-D,E). A statistical analysis of randomly sectioned bbs also revealed that cartwheels consist of two to seven tiers. The number of cartwheel tiers was analysed in 236 longitudinal sections of bbs; 99 bbs (41.9%) exhibited a cartwheel consisting of three tiers and 99 bbs (41.9%) a cartwheel consisting of four tiers. Only 11 bbs (4.7%) showed a cartwheel with only two tiers, 22 bbs (9.3%) a cartwheel with five tiers, three bbs (1.3%) a cartwheel with six tiers and two bbs (0.9%) a cartwheel with seven tiers (Fig. 3A-D,E).

In median longitudinal sections of the bb, a series of projections extend about 25 nm into the lumen of the bb (Fig. 1K, between two pairs of dashes) (Cavalier-Smith, 1974). They start about 25 nm (n=5) distal to the cartwheel and extend for about 215 nm (n=5) along the microtubular triplets. These structures were initially described as projections attached to the A-tubules and named 'A-tubule feet' (Cavalier-Smith, 1974). Our data show that these projections are associated with both the A- and B-tubules of each triplet (Fig. 4A-C, small arrowheads) and are interconnected by a very fine filament (Fig. 4A-C, small arrow). However, in preparations of isolated cytoskeletons fixed in the absence of tannic acid, the fine structure of the A-tubule feet is more complex (S. Geimer and M. Melkonian, unpublished). Similar projections attached to the microtubular triplets are also present in mammalian centrioles (Stubblefield and Brinkley, 1967; Ross, 1968; Paintrand et al., 1992).

The lumen of the bb is filled with filaments (Fig. 3A-C,E) of which some are attached to the A-tubule feet (Fig. 1H). In some micrographs the bb lumen appears to be empty, presumably because the filamentous material was extracted during isolation of the cytoskeletons (Fig. 1I-K, Fig. 4A-C).

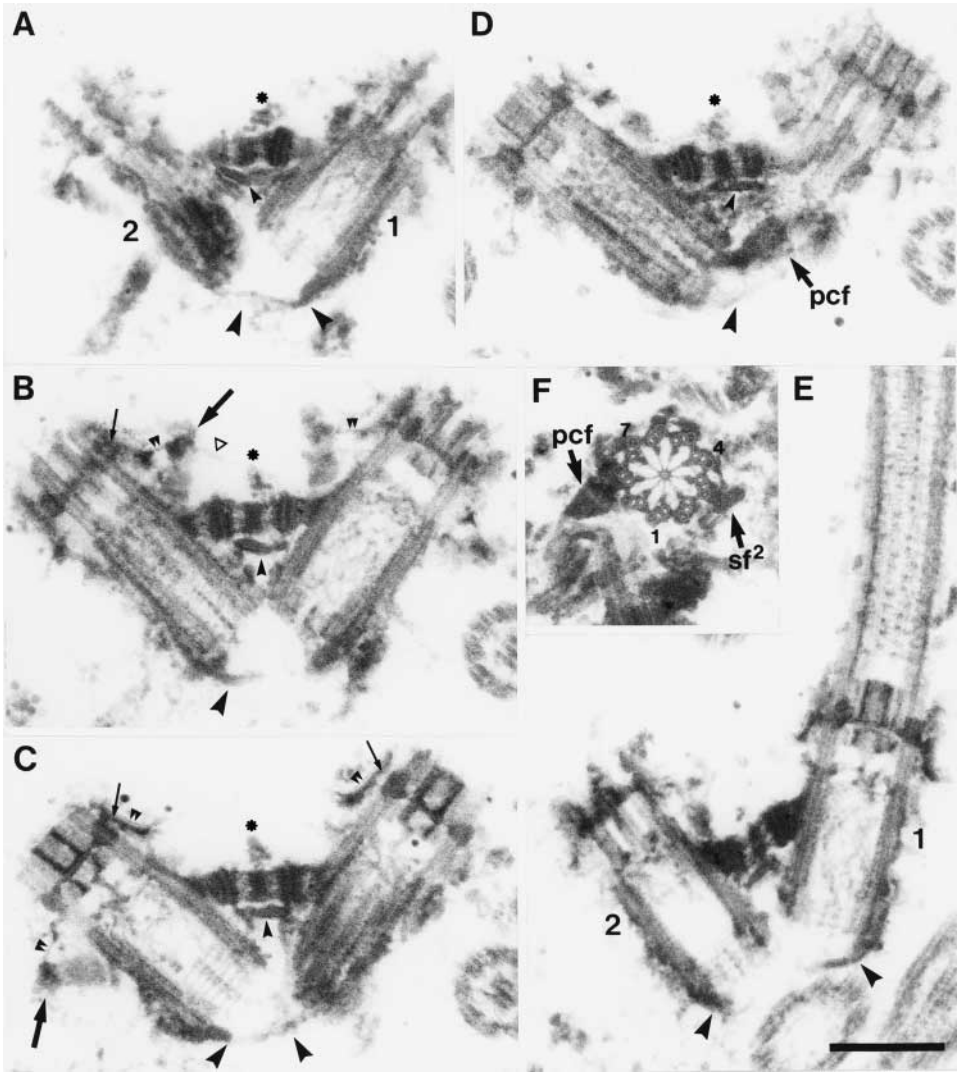

Fig. 3. The older and younger basal bodies. (A-D) Consecutive longitudinal sections through a basal apparatus. The cartwheel of the right bb consists of four tiers (A) and so this bb is assumed to be the developmentally older (A, 1), whereas the cartwheel of the left bb consists of seven tiers (C) and so this bb is assumed to be developmentally younger (A, 2). Membrane fragments (B,C, double arrowheads) associated with the doublet outer projections (B,C, small arrows) make contact with the distal end of the transitional fibers (B,C, large arrows). Above the center of the distal connecting fiber, a triangular structure is visible (A-D, asterisks) that is connected by a fine filament to the distal end of at least the transitional fiber attached to triplet 9 (B, open triangle). Lying below the dcf, the SMAFs (A-D, small arrowheads) seem to form a continuous fiber in the center region of the basal apparatus (B,C, small arrowheads) and are connected to the outer bands of the dcf by fine filaments (visible in C). The median proximal connecting fiber (A-D, large arrowheads) and the proximal connecting fiber of bb 2 (D, pcf) are visible. (E) Longitudinal section through a basal apparatus (the bbs are numbered). The cartwheel of bb 1 consist of three tiers, whereas the cartwheel of bb 2 exhibits four tiers. The complex system of filaments present in the lumen of the bbs is clearly visible in bb 1 and seems to be more dense in bb 1 than in bb 2. This is also the case for the bbs shown in A-D. (F) Transverse section through the proximal end of a bb showing the hub and spoke complex of the cartwheel (triplet numbers are indicated). Parts of the pcf and sf^2 are visible. Notice that the C-tubules are filled with electron-dense material. Scale bar, 250 nm.

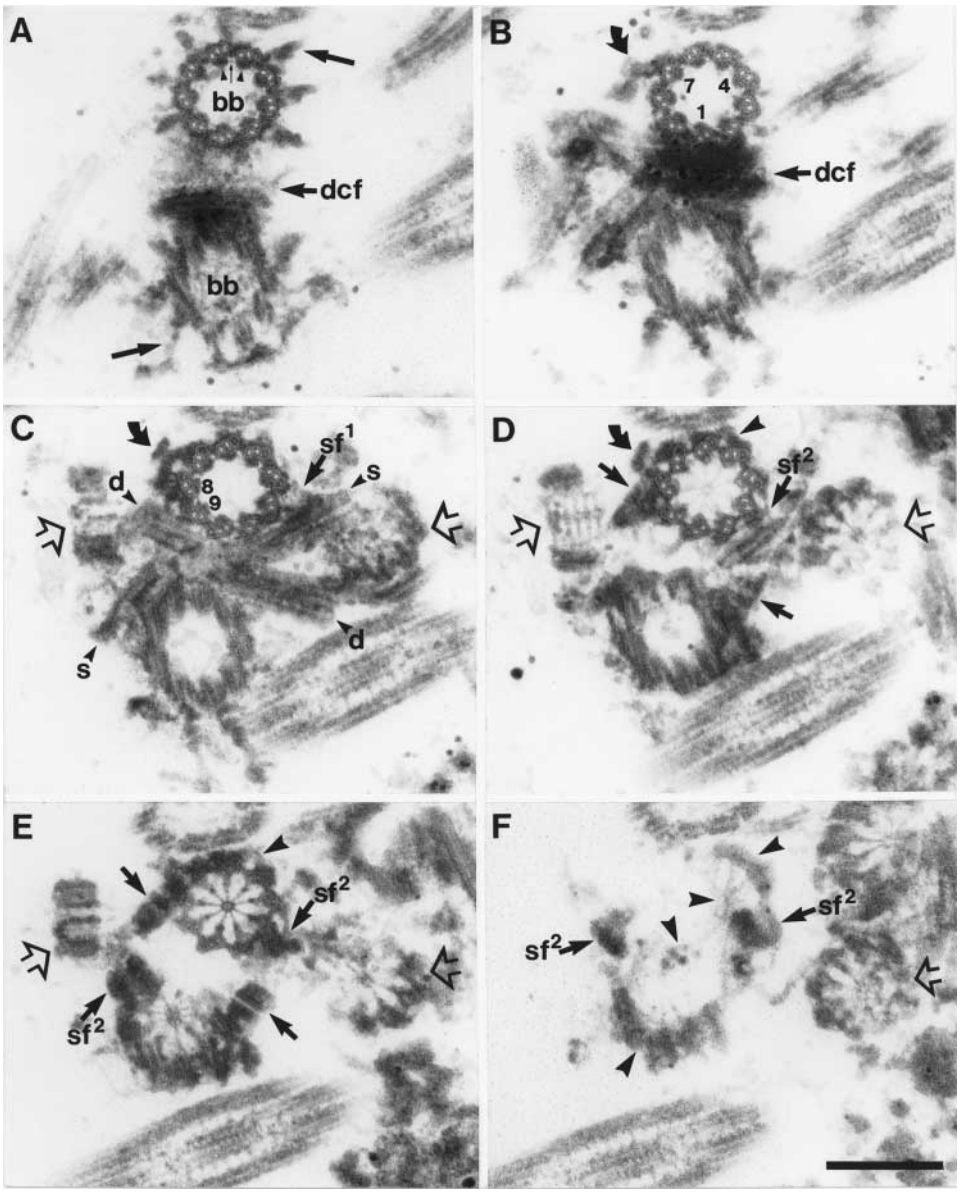

Fig. 4. Consecutive transverse sections through the basal apparatus showing the two bbs (A; the upper bb is sectioned transversely, the lower bb at an oblique angle) and probasal bodies (C-F, open arrows; the left pbb is sectioned longitudinally, the right pbb transversely). Within the lumen of the bb, electron-dense patches are associated with the A- and B-tubules of the microtubular triplets (A, small arrowheads; see also Fig. 1K). These patches are interconnected by a fine filament (A, small arrow). The distal connecting fiber (A,B, dcf) is attached to triplets 9, 1 and 2 of each bb, starting at the level where the transitional fibers (A, large arrows) terminate. The nucleus-bb connector is attached to triplets 7 and 8 (B-D, curved arrows). The cruciate microtubular root system is labeled in C [d for the dexter (right) roots, s for the sinister (left) roots]. The s-roots are connected to the bbs by two sets of fibers: the more distal sf^1 is attached to the C-tubule of triplet 4 (C, sf^1) and makes contact with the upper surface of the corresponding s-root; the more proximal sf^2 (D-F, sf^2) makes contact with the lower surface of the corresponding s-root. The main attachment site of the sf^2 with the bb is triplet 3, but projections are also in contact with triplets 2 and 4 (see also Fig. 3F). Material of the sf^2 is underlying at least triplets 2 and 3 below the proximal end of the bbs (F, sf^2). The d-roots are linked to the bbs by the d-fibers; the df is attached to triplets 8 and 9 (C, triplets numbered). At their proximal ends, the bbs are interconnected by two proximal connecting fibers and a median proximal connecting fiber. The main attachment site of the proximal connecting fiber (D,E, arrows) is triplet 8, but it also makes contact with triplets 7 and 9 (see also Fig. 3F). Attachment sides of the median proximal connecting fiber are, more distal at the bb, triplets 5 and 6 (D,E, arrowheads); more proximal at the bb, the mpcf is also attached to triplets 4, 7 and 8. Parts of the median proximal connecting fiber underlying the proximal ends of the bbs are visible in F (arrowheads, see also Fig. 3A-D). For the proximal connecting fibers and median proximal connecting fibers, see also Fig. 6I,J. Scale bar, 250 nm.

Probasal bodies

The probasal bodies (pbbs) are – like the flagella-bearing bbs – composed of nine microtubular triplets with connections between the A- and C-tubules of adjacent triplets (Fig. 2B) (Ringo, 1967; O'Toole et al., 2003). The microtubular triplets were complete in all observed pbbs (*n*=20), the B- and C-tubules are filled with electron-dense material (Fig. 2B). The pbbs have an average length of 95 nm (*n*=10), based on the length of the microtubular triplets, and their diameter is the same as that of the bbs (about 210 nm, *n*=10).

It has previously been shown for other flagellate green algae that the number of cartwheel tiers in the pbbs is higher than in the bbs (Beech et al., 1991). This is also true for *Chlamydomonas* – a statistical analysis of 53 longitudinal sections of pbbs revealed that the cartwheel of the pbb consists of four to seven tiers. Of the 53 pbbs analysed, 23 (43.4%) exhibited a cartwheel consisting of five tiers, 17 (32.1%) a cartwheel with four tiers, 12 (22.6%) a cartwheel with six tiers and only one pbb (1.9%) a cartwheel with seven tiers. Only three or four tiers are embedded in the microtubular cylinder (Fig. 2F, Fig. 5E) and the cartwheel protrudes proximally from the microtubular triplets in a conical shape; that is, the diameter of the tiers decreases gradually (Fig. 2F, open arrow).

The position of the acorn (see above) in the pbb allows the introduction of a tentative numbering system for the pbb

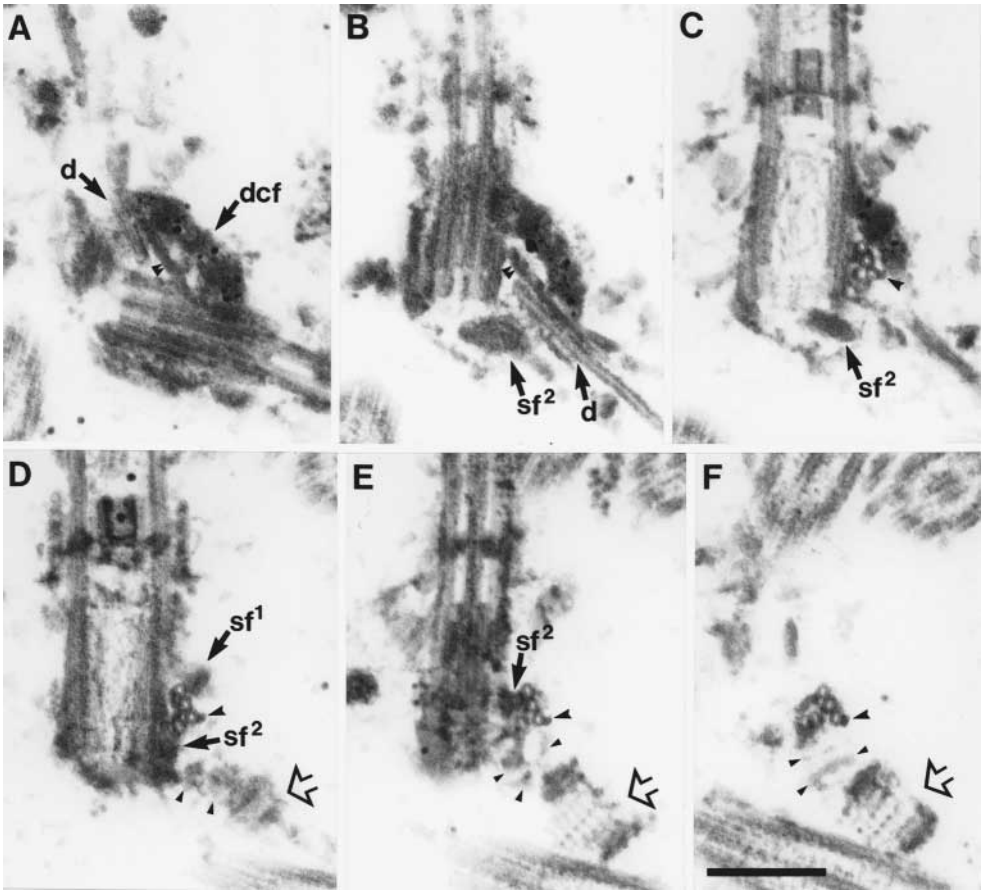

Fig. 5. Consecutive series showing the d- and s-roots, SMAFs and pbb. (A,B) The distal connecting fiber (dcf), both d-roots (d; their proximal ends are visible) and the corresponding SMAFs (double arrowheads) are marked. Notice that, at their proximal ends, the d-root microtubules are detached from their corresponding SMAFs. (C-F) The s-root in transverse sections. The SMAF (C-F, large arrowheads) overlying the s-root is very small and only associated with root microtubule 4. Near the proximal end of the s-root, microtubules 2 and 3 are attached by some electron-dense material to the bb (C). The sf^1 (D, sf^1) is attached to the upper surface of the s-root to root microtubules 2 and 3. The sf^2 (D,E, sf^2) makes contact with the lower surface of the s-root to root microtubules 1, 2 and 3. Material of the sf^2 is underlying the bb (B,C, sf^2). Filaments of the lateral striated fiber interconnecting the pbb (D-F, open arrows) to the sf^2, the s-root microtubules and probably the bb proper are labeled (D-F, small arrowheads). Scale bar, 250 nm.

triplets (Fig. 2B, see also Fig. 7G,H). Based on this observation, we estimate that pbbs are rotated by 140° with respect to the flagella-bearing bbs with which they are distributed to progeny during cell division (Fig. 7G,H).

Transitional region

About 50 nm (*n*=5) distal to the end of the C-microtubules of the bb, there is a transitional region (tr) characteristic for green flagellates. The tr contains two distinct stellate structures that are separated by the transitional plate (tp) (Fig. 1C-F,K, tr) (Ringo, 1967; O'Toole et al., 2003). The stellate structure is formed by filaments that connect the A-tubules of every third axonemal doublet with each other, constituting (as seen in transverse sections) a nine-pointed star with a central ring-like hub (Fig. 1D,F) In the distal stellate structure, the hub is lined with electron-dense material that is not present in the proximal stellate structure (compare Fig. 1D with 1F). In longitudinal sections, the two stellate structures form an H-piece made up of the distal (about 95 nm long) and the shorter proximal (about 55 nm long) stellate structure, and separated by the tp (Fig. 1K, tr). As typical for chlorophycean algae (Melkonian, 1984), the proximal end of the distal stellate structure is attached to and closed by the tp, which extends to the microtubular doublets (Fig. 1K, Fig. 2G, Fig. 3C,E). The distal end of the proximal stellate structure is not attached to the tp but is closed by a second plate, which, unlike the tp, does not extend to the microtubular doublets (Fig. 2G, Fig. 3E, bb1). This plate has not been observed in previous studies, presumably because it is sometimes closely appressed to the tp and thus not discernible (Fig. 1K, Fig. 3C). Cross sections of the tp have previously not been documented in conventional thin sections, but they were shown in a recent study using dual-axis electron tomography to be a central, amorphous disk (O'Toole et al., 2003). In our preparations, the central, amorphous disk is also revealed (Fig. 1E). However, the tp clearly extends between the microtubular doublets into the doublet outer projections (see below), which, at this level, form saw tooth-like structures projecting from the microtubular cylinder (Fig. 1E, compare with Fig. 1K showing the tp in longitudinal section).

Doublet outer projections

In the area of the tr, each of the nine doublets bears a short (about 40-50 nm) T-shaped fiber termed the 'doublet outer projection' (Cavalier-Smith, 1974), which is attached to the A/B-tubule junction (Fig. 1C,D,F, small arrows). In longitudinal sections, the doublet outer projections form two discrete zones of wedge-shaped, dense material (Fig. 1K, small arrows). In cross sections through the proximal stellate structure, the doublet outer projections are sometimes interconnected, forming a ring (Fig. 1F, small arrows). Membrane fragments attached to the doublet outer projections can be seen making contact with the distal end of the transitional fibers (Fig. 3B,C, double arrowheads).

Transitional fibers

The transitional fibers (tfs) were first described by Ringo (Ringo, 1967). In cross sections of the bb, they project radially counterclockwise from each triplet. The tfs are about 170 nm in length and have a swollen distal end (Fig. 1G, Fig. 2D,E, large arrows). They are attached to the distal third of the bb over a region of about 120 nm (Fig. 1G-I,K, large arrows). The tfs show a faint striation pattern (Fig. 1K, Fig. 3C) but, as in cryofixed cells (O'Toole et al., 2003), the exact number and spacing of the cross-striations are difficult to determine. The swollen distal ends of the transitional fibers are interconnected by a fine filament (not shown) and a fine filament runs from the distal end of at least the transitional fiber attached to triplet 9 to a triangular structure located above the center of the dcf (Fig. 3B, open triangle and asterisk).

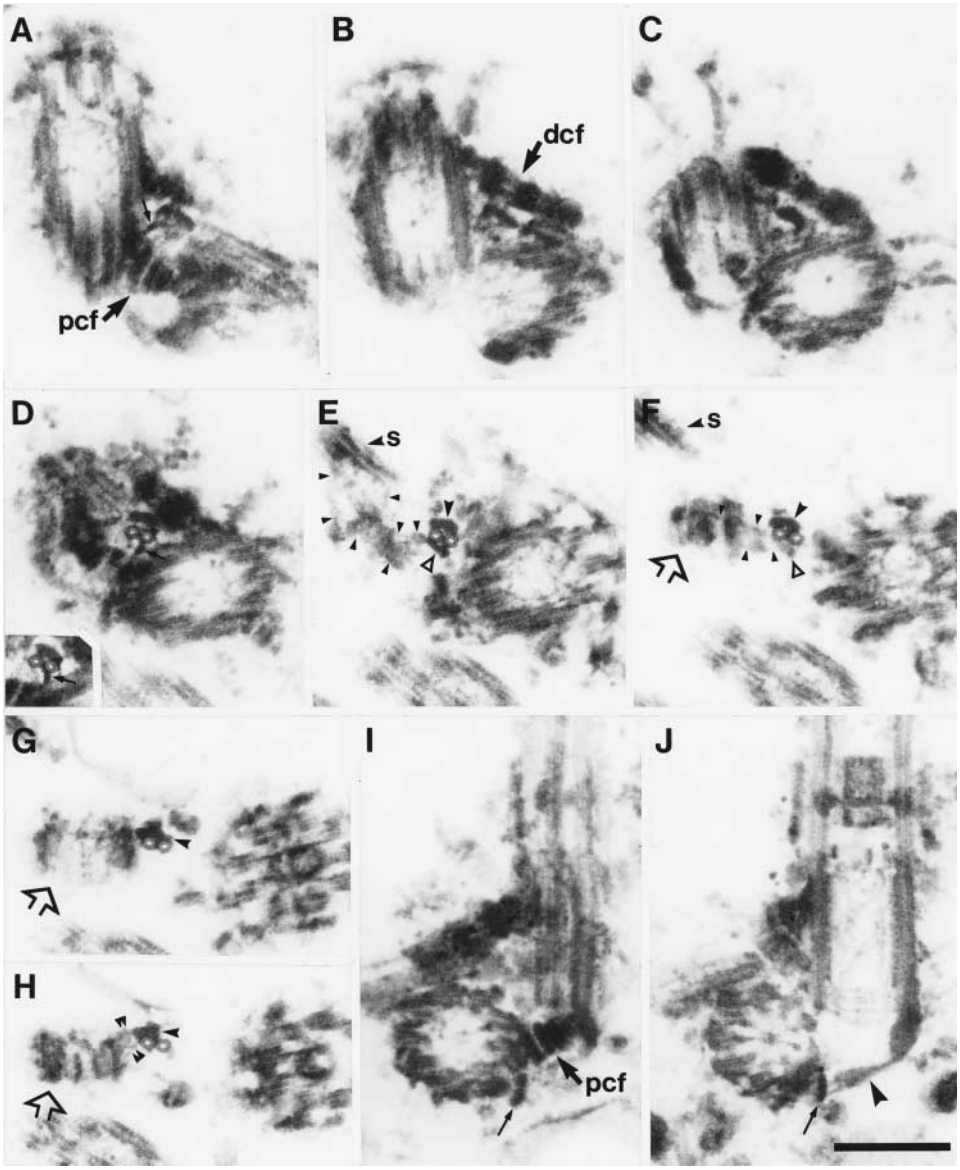

Fig. 6. The d-root, SMAFs, pbb and proximal connecting fibers. (A-H) Consecutive series showing the d-root in transverse section. The two bbs are sectioned at an oblique angle and the pbb is sectioned longitudinally. (A,B) The distal connecting fiber (B, dcf) and one proximal connecting fiber (A, pcf) are marked. The d-root is linked to the corresponding bb by the df (A,D and inset in D, small arrows). In the more proximal region of the d-root, the corresponding SMAF (E-H, large arrowheads) is overlying both root microtubules (D-G), whereas, more distally, it is overlying only root microtubule 2 (H). The striation pattern of the SMAF is clearly visible in F and G. (E,F) The pbb is connected to the d-root by the lateral striated fiber (see also Fig. 2C,H, large arrowheads). Filaments of the lateral striated fiber (E,F, small arrowheads) extend from an electron-dense plate underlying both microtubules of the d-root (E,F, open triangles) to the side of the pbb (F, open arrow), and some of these filaments (E, small arrowheads) seem also to be connected to the s-root (E,F, s). More distal at the d-root, filamentous material interconnects the pbb with the SMAF (H, double arrowheads). (I,J) Two consecutive serial sections showing the two sets of proximal connecting fibers. The left bb is seen in transverse, the right in longitudinal section. The proximal connecting fiber (I, pcf) shows a complex cross striation. The median proximal connecting fiber (J, arrowhead) is not cross striated and is attached to a hook-like structure (I,J, small arrow). Scale bar, 250 nm.

Connections between the flagella-bearing bbs and the microtubular flagellar roots

An array of morphologically distinct fibers link specific bb triplets to the microtubular flagellar roots. Two sets of fibers extend laterally from each bb: left fibers (sf^1 and sf^2) connecting the bb to the four-stranded microtubular root (s-root), and the right fiber (df) connecting the bb to the two-stranded microtubular root (d-root). The spatial arrangement of these fibers within the basal apparatus is illustrated in Fig. 7.

The sf^1 is attached to the mid-region, the sf^2 to the more proximal region of the bb (Fig. 5D, sf^1 and sf^2). The fan-shaped sf^1 arises from the C-tubule of triplet 4 and traverses about 90 nm (Fig. 4C, sf^1) to contact the upper surface of the corresponding s-root (root microtubules 2 and 3; Fig. 5D, see also Fig. 7G, sf^1). The sf^2 is mainly attached to triplet 3 but projections are also in contact with triplets 2 and 4. It traverses about 45 nm (Fig. 4D,E, sf^2) and contacts the lower surface of the corresponding s-root (root microtubules 1, 2 and 3; Fig. 5D,E, Fig. 7H, sf^2). The sf^2 extends to the most proximal end of the bb and underlies at least triplets 2 and 3 (Fig. 4F, Fig. 5B,C, Fig. 7I, sf^2).

The df is attached to triplets 8 and 9 (Fig. 4C, triplets 8 and 9 numbered, see also Fig. 7G, df) and extends about 30 nm to contact the lower surface of the corresponding d-root (with root microtubule 1; Fig. 6D and inset, small arrows).

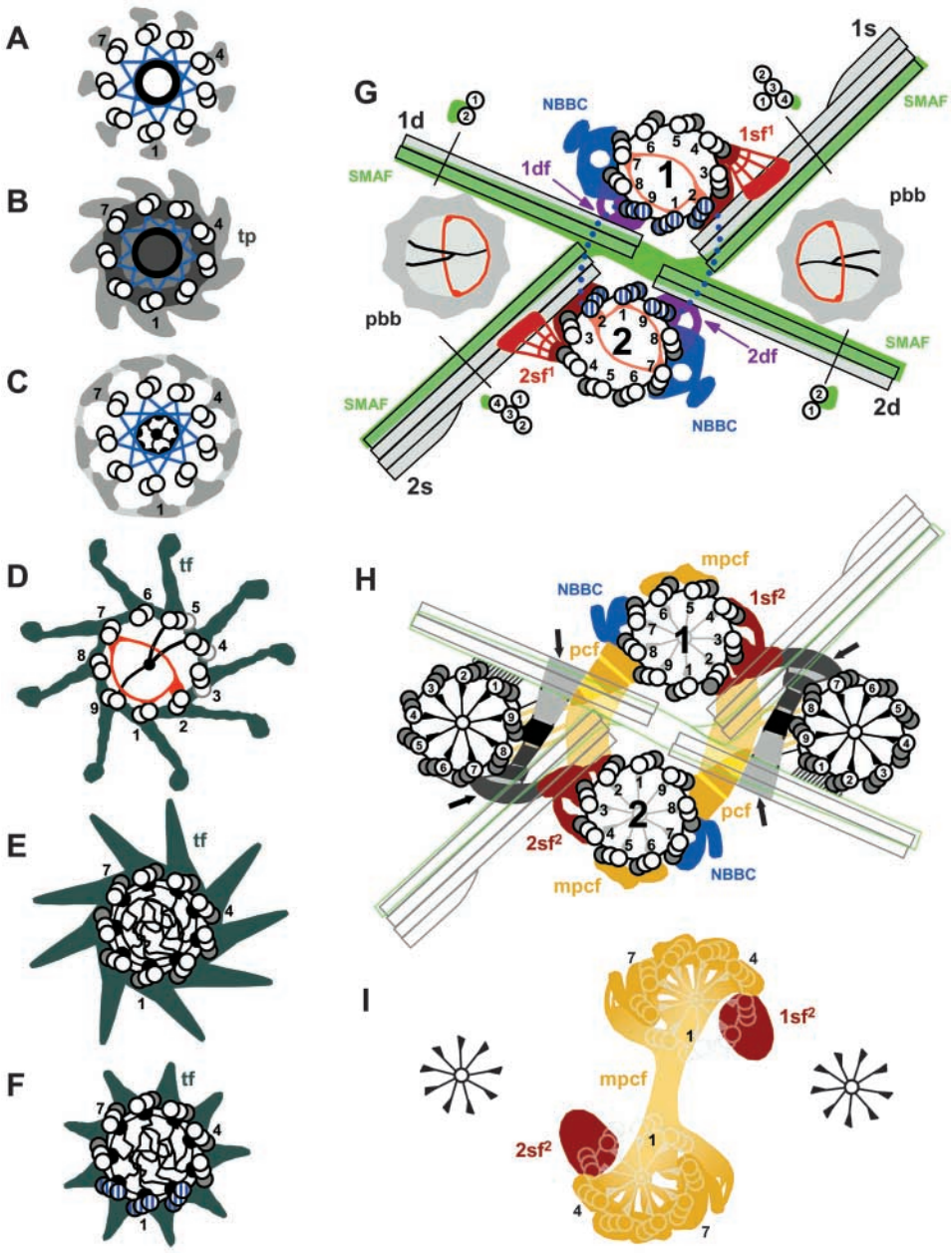

Fig. 7. The basal apparatus of *Chlamydomonas reinhardtii* (transverse sections, from distal to proximal, doublets/triplets are numbered). (A-F) The transitional region and distal part of a bb. Centrin-containing filaments are depicted in blue and triplets to which the dcf is attached are filled with blue stripes. (A-C) The transitional region. The doublet outer projections attached to the A/B-tubule junction at the outside of the doublets are shown in light gray. (B) The region containing the transitional plate (tp). (D-F) Transition between transitional region and bb, and distal part of the bb with the attached transitional fibers (tf, dark green). (D) Filaments are attached in an asymmetrical way at the inner surface of the microtubular cylinder exactly at the transition between transitional region and bb. A filament outlining the shape of an acorn (red) is attached to doublets (rarely triplets) 7, 8, 9, 1 and 2. The lumenal side of the acorn is crossed by a V-shaped filament system; two filaments extend from triplets 4 and 5 to fuse in the center of the bb lumen and continue to the other side of the bb, making contact with triplet 9. The acorn and V-shaped filament system are already present at the distal end of the pbbs (G, pbb). (G-I) The bb root complex. (G) Median part of the bb root complex at a level where the microtubular roots and striated microtubule associated fibers (SMAFs) are present. The distal connecting fiber has been omitted for clarity but its position is outlined by dotted blue lines and the triplets to which the dcf is attached are filled with blue stripes. At this level, the acorn is actually not present in the bb but it is given in this schematic diagram for a better understanding of its positional relationship with the other elements of the basal apparatus. The cruciate microtubular roots are labeled 1d, 1s, 2d and 2s. Each microtubular root is associated with a SMAF, which are shown in green. The microtubular roots and SMAFs are also shown in cross sectional view, with individual root microtubules numbered. The first set of s-fibers ($1sf^1$, $2sf^1$) connecting the bbs to their corresponding four-stranded microtubular roots (s-roots, 1s, 2s) are shown in red. The d-fibers (1df, 2df) that interconnect the bbs with their corresponding two-stranded microtubular roots (d-roots, 1d, 2d) are given in purple. The nucleus-bb connectors (NBBC, blue) are seen attached to the bbs in this region. At the distal ends of the pbbs (pbb, shades of gray) the acorn (red) and the V-shaped filament system are present (compare with D). (H) Proximal part of the bb root complex at a level below the microtubular roots and SMAFs (for a better orientation outlined in gray and green, respectively). The second set of s-fibers ($1sf^2$, $2sf^2$) connecting the bbs to their corresponding four-stranded microtubular roots (s-roots, 1s, 2s) is shown in red. The proximal connecting fibers (pcf, yellow) interconnect the bbs and also make contact with the adjacent pbb (with pbb triplets 8 and 9). The pbbs (their microtubular triplets are numbered) are attached by the lateral striated fiber (arrows) to their corresponding d-root and the sf^2 of the neighboring bb. In this region, the median proximal connecting fiber is attached to triplets 5 and 6 (mpcf, yellow). (I) Structures lying below the proximal ends of the bbs (faintly outlined) are the median proximal connecting fiber (mpcf, yellow) and the proximal parts of the sf^2 (red). Of the pbbs, only the hub and spoke complex of the cartwheels are visible at this level.

Connections between the pbbs and bbs, microtubular roots and striated microtubule-associated fibers

The pbbs are connected to the bbs, the d-roots and their corresponding striated microtubule-associated fibers (SMAFs), and the s-roots by different fibers, and we describe the attachment of these fibers to particular triplets of the pbb (Fig. 7H). In cross sections through the basal apparatus, a striated fiber originates at a d-root mid-way between the pbb and a bb,

extends about 280 nm towards the pbb, and then passes between the pbb and the opposite bb (Fig. 2B,C,H, large arrowheads; Fig. 7H, arrows). This fiber was first observed and termed 'lateral striated fiber' (lsf) by Weiss (Weiss, 1984). The lsf shows a cross-striation pattern consisting of electron-dense bands of about 30-45 nm that are separated by electron-translucent areas of about 10-20 nm and is attached to pbb triplets 7, 8 and 9 (Fig. 2B,C,H). In cross sections of the d-root, the lsf (Fig. 6E,F, small arrowheads) attaches to an electron-dense plate underlying both root microtubules (Fig. 6E,F, open triangles). Filaments of the lsf (Fig. 5D-F, Fig. 6E, small arrowheads) continue to the sf^2 (Fig. 5D,E, sf^2) and the s-root (Fig. 6E, s). The pbb is linked to the d-root at a second site by thin filaments extending from the SMAF overlying the d-root to triplets 1 and 2 of the pbb (Fig. 2B, Fig. 6H, double arrowheads). A direct connection between a flagella-bearing bb and a pbb is made by material of the proximal connecting fiber (Fig. 4D,E) contacting pbb triplets 8 and 9 (Fig. 7H).

Proximal connecting fibers

Previously, only two cross-striated proximal connecting fibers (pcfs) had been described attached to the bbs (Ringo, 1967). The two pcfs are linked to triplets 8 and 9 (Fig. 2H, pcf, Fig. 3F, pcf, Fig. 4D,E, arrows). The connection of the pcf to triplets 2 and 3 of the opposing bb is made through the sf^2 (Fig. 2H, Fig. 4E). In this study an additional pcf was detected. A similar fiber had been previously described in zoospores of the green alga *Chlorosarcinopsis* and termed a 'median pcf' (mpcf) (Melkonian, 1978) (Fig. 3A-D, Fig. 4F, Fig. 6J, large arrowheads). The mpcf is not cross-striated and, at its distal end, is attached to triplets 5 and 6 (Fig. 4D, large arrowhead), whereas, more proximally, it is linked to triplets 4, 5, 6, 7 and 8 (Fig. 4E,F, large arrowheads). At triplet 8, the mpcf is attached to a hook-like structure (Fig. 6J, small arrow). Material of the mpcf underlies the proximal ends of the bb (Fig. 3A-D,E, Fig. 6J, large arrowheads) and forms, together with parts of the sf^2, an electron-dense, open ring (Fig. 4F).

Discussion

Ultrastructure of the *C. reinhardtii* basal apparatus revisited

The ultrastructure of the basal apparatus of *C. reinhardtii* has been analysed in detail by serial ultrathin section electron microscopy of isolated cytoskeletons. New information has been presented on the structure of the pcfs, the fibers connecting the bb with the microtubular flagellar roots, the linkage of the pbbs to other elements of the basal apparatus and the bbs/pbbs themselves. These data will facilitate the precise mapping of previously identified as well as novel basal apparatus proteins, the prediction of possible protein-protein interactions and the analysis of mutants and RNA interference cells with only subtle defects in structural components of the basal apparatus.

The high density of basal apparatuses in our preparations made it possible to statistically analyse a large number of basal apparatuses. The diagram illustrating the basal apparatus ultrastructure (Fig. 7) is based on data derived from the analysis of 60 complete series and several hundred non-serial sections through basal apparatuses. An important issue when studying subcellular structures is whether or not the isolation procedure has led to structural modifications. Information about the ultrastructure of the basal apparatus of *C. reinhardtii* in situ has been provided previously (Ringo, 1967; Johnson and Porter, 1968; Cavalier-Smith, 1974; Goodenough and Weiss, 1978; Hoops and Witman, 1983; Weiss, 1984; Gaffal, 1988; O'Toole et al., 2003). Careful comparison of these data with our own findings leads us to conclude that the basal apparatuses that we have analysed were structurally intact.

Using this approach, several novel basal apparatus structures were identified during this study. Three types of specialized fibers were identified that link the microtubular flagellar roots directly to particular triplets of the basal bodies. The four-stranded microtubular roots (s-roots) are attached to the basal bodies by two sets of s-fibers (sf^1 and sf^2) and the two-stranded microtubular roots (d-roots) by the d-fibers (df). These fibers are predominantly associated with the C-tubules of the respective triplets (e.g. the sf^1 is exclusively linked to the C-tubule of triplet 4). For the related flagellate green alga *S. similis*, it has also been shown that the B- and (in particular) the C-tubules are the preferred attachment sites for bb-associated structures (Geimer et al., 1997).

Structural marker for the rotational polarity is inherent in bbs and pbbs

The most significant single observation made during this study was the discovery of a structural component, the acorn, that confers rotational asymmetry on both bbs and pbbs. It has been previously noted that ciliary and flagellar basal bodies display axial as well as rotational polarities (e.g. Anderson and Brenner, 1971; Hoops and Witman, 1983; Sandoz et al., 1988; Beech and Melkonian, 1993; Geimer et al., 1997) (reviewed in Beisson and Jerka-Dziadosz, 1999). A marker for the axial polarity of bbs and centrioles is the highly conserved cartwheel, which is attached to the inner wall of the microtubular cylinder at its proximal end. The rotational polarity of basal bodies previously could only be inferred indirectly from the asymmetric association of various fibers and/or microtubules to specific bb triplets at the outside of the microtubular cylinder. Here, we describe a structural marker for the rotational asymmetry inherent in the bbs and pbbs: at the most distal end of the microtubular cylinder, a fiber outlining the shape of an acorn is attached to triplets 7, 8, 9, 1 and 2. This structure can also be recognized in intact cells in published micrographs [see Fig. 36 (Ringo, 1967); see supplemental videos (O'Toole et al., 2003)].

The ultrastructural data presented here show that the distal end of the pbb is already highly specialized. Other than tubulin, few proteins have been localized to pbbs. In the flagellate green alga *S. similis*, p210 (a component of the doublet outer projections in the tr), was localized to an asymmetric pattern at the distal end of the pbbs soon after their assembly (Lechtreck and Grunow, 1999). Centrin is also found in the pbbs of *S. similis* (Lechtreck and Grunow, 1999) and, in mammalian cells, centrin was detected at the site of procentriole formation even before tubulin was present (Middendorp et al., 1997). In *Chlamydomonas*, a kinesin-II protein, FLA10p (also called KHP1), is present at the pbbs (Vashishtha et al., 1996) and VFL1p, which is located within the lumen of bbs, was also shown to be present at the pbbs (Silflow et al., 2001). In the *Chlamydomonas vfl1* mutant

(Adams et al., 1985), the correct rotational orientation of the bbs is impaired (Silflow et al., 2001). By careful immunogold electron microscopy, Silflow et al. showed that the position of VFL1p in the basal body is rotationally asymmetric. VFL1p localizes to the most distal end of the bb near the microtubular triplets/doublets that face the dcf (triplets/doublets 9, 1 and 2) (Silflow et al., 2001). This localization corresponds well with the position of the acorn described here and suggests that VFL1p might be a component of this structure.

The acorn might play a role in targeting the assembly of various bb-associated fibers to specific triplets

The asymmetric position of the acorn within the microtubular cylinder suggests to us that the acorn might play a role during probasal body maturation by controlling the asymmetric assembly of the various bb-associated fibers. Defects in or absence of the acorn could disturb the highly specific spatial pattern of the fibers attached to the bbs. The triplets to which the acorn is attached are the same triplets to which the centrin-containing fibers of the nucleus-bb connector (triplets 7, 8) (Salisbury et al., 1988) and the dcf (triplets 9, 1, 2) (Hoops and Witman, 1983) are attached (Fig. 7). In *vfl1*, the dcf is either absent or incomplete (Adams et al., 1985). Mispositioned or absent s- and d-fibers would probably result in a mispositioning of the microtubular roots. This is the case in *vfl1* mutants, in which the normal cruciate array of microtubular flagellar roots has not been observed (Adams et al., 1985). In *vfl1* mutants, cell motility is also severely impaired, with even biflagellate cells showing aberrant spinning or tumbling movements, indicating that the flagella do not beat in opposite directions (Adams et al., 1985).

Is an acorn fiber a universal feature of the eukaryotic bb?

Basal bodies have been shown to express intrinsic and autonomous polarities. During the development of the oral apparatus in the ciliates *Tetrahymena* and *Stentor*, bbs first proliferate and lie at random positions, but their appendages develop at a predetermined site (Williams and Frankel, 1973; Paulin and Bussey, 1971) (reviewed in Beisson and Jerka-Dziadosz, 1999). An analogous situation was described for bbs in the nasal epithelium of mouse embryos (Frisch and Farbman, 1968). The analysis of a *Chlamydomonas vfl* mutant (*vfl3*) affecting the proper positioning of the pbbs has led to the hypothesis that the bbs have an intrinsic rotational polarity (Wright et al., 1983).

To address the question of whether acorn-like structures are a universal feature of bbs/centrioles in eukaryotic cells, we performed an exhaustive literature search. An acorn-type structure attached to five or six bb triplets is visible at the distal end of bbs in the green flagellate *S. similis* [(Geimer et al., 1997) Fig. 3], in the parabasalid protist *Pseudotrichonympha*, [(Gibbons and Grimstone, 1960) plate 351, Fig. 7] and in the chytridiomycete fungus *Phlyctochytrium irregulare* Koch [(McNitt, 1974) Fig. 3]. Thus, acorn-type structures apparently occur in three different eukaryotic kingdoms.

Does an acorn fiber occur in mammalian centrioles?

In Bornens (Bornens, 1992), a cross section of a human (lymphoblast) centriole is shown in which an acorn-type fiber can be seen apparently attached to five triplets. Stubblefield and Brinkley (Stubblefield and Brinkley, 1967) described a structure in the distal lumen in centrioles in Chinese hamster fibroblasts that did not exhibit ninefold rotational symmetry. Vorobjev and Chentsov (Vorobjev and Chentsov, 1980) found a fine filament that formed an incomplete circle at the distal end of centrioles in various mammalian species. In the latter two studies, the acorn is not clearly revealed. However, internal structures in the centriole/bb of mammalian cells have always been ill-defined, which might be related to their susceptibility to divalent cations (Paintrand et al., 1992). The acorn was even overlooked for a long time in the otherwise well-characterized bb of *Chlamydomonas*. We conclude that the acorn might be the long-sought-after structural equivalent of the cartwheel at the distal end of bbs/centrioles, providing rotational asymmetry to this enigmatic constituent of eukaryotic cells.

This study was supported by the Deutsche Forschungsgemeinschaft (Me 658/22-1).

References

Adams, G. M., Wright, R. L. and Jarvik, J. W. (1985). Defective temporal and spatial control of flagellar assembly in a mutant of *Chlamydomonas reinhardtii* with variable flagellar number. *J. Cell Biol.* **100**, 955-964.

Andersen, R. A., Barr, D. J. S., Lynn, D. H., Melkonian, M., Moestrup, Ø. and Sleigh, M. A. (1991). Terminology and nomenclature of the cytoskeletal elements associated with the flagellar/ciliary apparatus in protists. *Protoplasma* **164**, 1-8.

Anderson, R. G. and Brenner, R. M. (1971). The formation of basal bodies (centrioles) in the Rhesus monkey oviduct. *J. Cell Biol.* **50**, 10-34.

Asamizu, E., Miura, K., Kucho, K., Inoue, Y., Fukuzawa, H., Ohyama, K., Nakamura, Y. and Tabata, S. (2000). Generation of expressed sequence tags from low-CO_2 and high-CO_2 adapted cells of *Chlamydomonas reinhardtii*. *DNA Res.* **7**, 305-307.

Asamizu, E., Nakamura, Y., Sato, S., Fukuzawa, H. and Tabata, S. (1999). A large scale structural analysis of cDNAs in a unicellular green alga, *Chlamydomonas reinhardtii*. I. Generation of 3433 non-redundant expressed sequence tags. *DNA Res.* **6**, 369-373.

Beech, P. L., Heimann, K. and Melkonian, M. (1991). Development of the flagellar apparatus during the cell cycle in unicellular algae. *Protoplasma* **164**, 23-37.

Beech, P. L. and Melkonian, M. (1993). The basal apparatus of the quadriflagellate *Spermatozopsis exsultans* (Chlorophyceae): numbering of basal body triplets reveals triplet individuality and developmental modifications. *J. Phycol.* **29**, 191-202.

Beisson, J. and Jerka-Dziadosz, M. (1999). Polarities of the centriolar structure: morphogenetic consequences. *Biol. Cell* **91**, 367-378.

Beisson, J. and Wright, M. (2003). Basal body/centriole assembly and continuity. *Curr. Opin. Cell Biol.* **15**, 96-104.

Bornens, M. (1992). What is a centrosome? In *The Centrosome* (ed. V. I. Kalnins), pp. 2-43. New York: Academic Press.

Cavalier-Smith, T. (1974). Basal body and flagellar development during the vegetative cell cycle and the sexual cycle of *Chlamydomonas reinhardii*. *J. Cell Sci.* **16**, 529-556.

Dutcher, S. K. (2003). Elucidation of basal body and centriole functions in *Chlamydomonas reinhardtii*. *Traffic* **4**, 443-451.

Dutcher, S. K. and Trabuco, E. C. (1998). The *UNI3* gene is required for assembly of basal bodies of *Chlamydomonas* and encodes delta-tubulin, a new member of the tubulin superfamily. *Mol. Biol. Cell* **9**, 1293-1308.

Frisch, D. and Farbman, A. I. (1968). Development of order during ciliogenesis. *Anat. Rec.* **162**, 221-232.

Fuhrmann, M., Oertel, W. and Hegemann, P. (1999). A synthetic gene coding for the green fluorescent protein (GFP) is a versatile reporter in *Chlamydomonas reinhardtii*. *Plant J.* **19**, 353-361.

Fuhrmann, M., Stahlberg, A., Govorunova, E., Rank, S. and Hegemann, P. (2001). The abundant retinal protein of the *Chlamydomonas* eye is not

the photoreceptor for phototaxis and photophobic responses. *J. Cell Sci.* **114**, 3857-3863.

Gaffal, K. P. (1988). The basal body-root complex of *Chlamydomonas reinhardtii* during mitosis. *Protoplasma* **143**, 118-129.

Geimer, S., Lechtreck, K.-F. and Melkonian, M. (1997). The cytoskeleton of naked green flagellate *Spermatozopsis similis* (Chlorophyta): analysis of isolated basal apparatuses in parallel configuration. *J. Phycol.* **33**, 241-253.

Geimer, S., Clees, J., Melkonian, M. and Lechtreck, K.-F. (1998a). A novel 95-kD protein is located in a linker between cytoplasmic microtubules and basal bodies in a green flagellate and forms striated filaments in vitro. *J. Cell Biol.* **140**, 1149-1158.

Geimer, S., Lechtreck, K.-F. and Melkonian, M. (1998b). A novel basal apparatus protein of 90 kD (BAp90) from flagellate green alga *Spermatozopsis similis* is a component of the proximal plates and identifies the d (dexter)-surface of the basal body. *Protist* **149**, 173-184.

Gibbons, I. R. and Grimstone, A. V. (1960). On flagellar structure in certain flagellates. *Biophys. Biochem. Cytol.* **7**, 697-716.

Goodenough, U. W. and Weiss, R. L. (1978). Interrelationships between microtubules, a striated fiber, and the gametic mating structure of *Chlamydomonas reinhardtii*. *J. Cell Biol.* **76**, 430-438.

Heimann, K., Reize, I. B. and Melkonian, M. (1989). The flagellar developmental cycle in algae: flagellar transformation in *Cyanophora paradoxa* (Glaucocystophyceae). *Protoplasma* **148**, 106-110.

Hoops, H. J. and Witman, G. B. (1983). Outer doublet heterogeneity reveals structural polarity related to beat direction in *Chlamydomonas* flagella. *J. Cell Biol.* **97**, 902-908.

Johnson, U. G. and Porter, K. R. (1968). Fine structure of cell division in *Chlamydomonas reinhardi*. Basal bodies and microtubules. *J. Cell Biol.* **38**, 403-425.

Koblenz, B., Schoppmeier, J., Grunow, A. and Lechtreck, K.-F. (2003). Centrin deficiency in *Chlamydomonas* causes defects in basal body replication, segregation and maturation. *J. Cell Sci.* **116**, 2635-2646.

Lechtreck, K.-F. and Grunow, A. (1999). Evidence for a direct role of nascent basal bodies during spindle pole initiation in the green alga *Spermatozopsis similis*. *Protist* **150**, 163-181.

Lechtreck, K.-F. and Melkonian, M. (1991). Striated microtubule-associated fibers: identification of assemblin, a novel 34-kD protein that forms paracrystals of 2-nm filaments in vitro. *J. Cell Biol.* **115**, 705-716.

Lechtreck, K.-F., Rostmann, J. and Grunow, A. (2002). Analysis of *Chlamydomonas* SF-assemblin by GFP tagging and expression of antisense constructs. *J. Cell Sci.* **115**, 1511-1522.

Lechtreck, K.-F., Teltenkötter, A. and Grunow, A. (1999). A 210 kDa protein is located in a membrane-microtubule linker at the distal end of mature and nascent basal bodies. *J. Cell Sci.* **112**, 1633-1644.

Marshall, W. F. and Rosenbaum, J. L. (2000). How centrioles work: lessons from green yeast. *Curr. Opin. Cell Biol.* **12**, 119-125.

McFadden, G. I. and Melkonian, M. (1986). Use of HEPES buffer for microalgal culture media and fixation for electron microscopy. *Phycologia* **25**, 551-557.

McNitt, R. (1974). Centriole ultrastructure and its possible role in microtubule formation in an aquatic fungus. *Protoplasma* **80**, 91-108.

Melkonian, M. (1978). Structure and significance of cruciate flagellar root systems in green algae: comparative investigations in species of *Chlorosarcinopsis* (Chlorosarcinales). *Plant Syst. Evol.* **130**, 265-292.

Melkonian, M. (1984). Flagellar apparatus ultrastructure in relation to green algal classification. In *Systematics of the Green Algae* (ed. D. E. G. Irvine and D. M. John), pp. 73-120. New York: Academic Press.

Middendorp, S., Paoletti, A., Schiebel, E. and Bornens, M. (1997). Identification of a new mammalian centrin gene, more closely related to *Saccharomyces cerevisiae CDC31* gene. *Proc. Natl. Acad. Sci. USA* **94**, 9141-9146.

Moestrup, Ø. and Hori, T. (1989). Ultrastructure of the flagellar apparatus in *Pyramimonas octopus* (Prasinophyceae) II. Flagellar roots, connecting fibres, and numbering of individual flagella in green algae. *Protoplasma* **148**, 41-56.

O'Toole, E. T., Giddings, T. H., McIntosh, J. R. and Dutcher, S. K. (2003). Three-dimensional organization of basal bodies from wild-type and δ-tubulin deletion strains of *Chlamydomonas reinhardtii*. *Mol. Biol. Cell* **14**, 2999-3012.

Paintrand, M., Moudjou, M., Delacroix, H. and Bornens, M. (1992). Centrosome organization and centriole architecture: their sensitivity to divalent cations. *J. Struct. Biol.* **108**, 107-128.

Paulin, J. J. and Bussey, J. (1971). Oral regeneration in the ciliate *Stentor coeruleus*: a scanning and transmission electron optical study. *J. Protozool.* **18**, 201-213.

Preble, A. M., Giddings, T. M., Jr and Dutcher, S. K. (2000). Basal bodies and centrioles: their function and structure. *Curr. Top. Dev. Biol.* **49**, 207-233.

Reynolds, E. S. (1963). Use of lead citrate at high pH as an electron-opaque stain in electron microscopy. *J. Cell Biol.* **17**, 208-212.

Ringo, D. L. (1967). Flagellar motion and fine structure of the flagellar apparatus in *Chlamydomonas*. *J. Cell Biol.* **33**, 543-571.

Ross, A. (1968). The substructure of centriole subfibers. *J. Ultrastruct. Res.* **23**, 537-539.

Ruiz-Binder, N. E., Geimer, S. and Melkonian, M. (2002). In vivo localization of centrin in the green alga *Chlamydomonas reinhardtii*. *Cell Motil. Cytoskeleton* **52**, 43-55.

Salisbury, J. L. (1995). Centrin, centrosomes, and mitotic spindle poles. *Curr. Opin. Cell Biol.* **7**, 39-45.

Salisbury, J. L., Baron, A. T. and Sanders, M. A. (1988). The centrin-based cytoskeleton of *Chlamydomonas reinhardtii*: distribution in interphase and mitotic cells. *J. Cell Biol.* **107**, 635-641.

Sandoz, D., Chailley, B., Boisvieux-Ulrich, E., Lemullois, M., Laine, M. C. and Bautista-Harris, G. (1988). Organization and functions of cytoskeleton in metazoan ciliated cells. *Biol. Cell* **63**, 183-193.

Schlösser, U. G. (1994). SAG – Sammlung von Algenkulturen at the University of Göttingen: catalogue of strains. *Bot. Acta* **107**, 113-186.

Shrager, J., Hauser, C., Chang, C. W., Harris, E. H., Davies, J., McDermott, J., Tamse, R., Zhang, Z. and Grossman, A. R. (2003). *Chlamydomonas reinhardtii* genome project. A guide to the generation and use of the cDNA information. *Plant Physiol.* **131**, 401-408.

Silflow, C. and Iyadurai, K. B. (2002). The *Chlamydomonas VFL3* gene product is required for correct positioning of the basal bodies. *Mol. Biol. Cell* **13 Suppl.**, 326a.

Silflow, C. D., LaVoie, M., Tam, L. W., Tousey, S., Sanders, M., Wu, W., Borodovsky, M. and Lefebvre, P. A. (2001). The Vfl1 protein in *Chlamydomonas* localizes in a rotationally asymmetric pattern at the distal ends of the basal bodies. *J. Cell Biol.* **153**, 63-74.

Stubblefield, E. and Brinkley, B. R. (1967). Architecture and function of the mammalian centriole. In *Formation and Fate of Cell Organelles* (ed. K. B. Warren), pp. 175-218. New York and London: Academic Press.

Vashishtha, M., Walther, Z. and Hall, J. L. (1996). The kinesin-homologous protein encoded by the *Chlamydomonas FLA10* gene is associated with basal bodies and centrioles. *J. Cell Sci.* **109**, 541-549.

Vorobjev, I. A. and Chentsov, Y. S. (1980). The ultrastructure of centriole in mammalian tissue culture cells. *Cell Biol. Int. Rep.* **4**, 1037-1044.

Weiss, R. L. (1984). Ultrastructure of the flagellar roots in *Chlamydomonas* gametes. *J. Cell Sci.* **67**, 133-143.

Williams, N. E. and Frankel, J. (1973). Regulation of microtubules in *Tetrahymena*. I. Electron microscopy of oral replacement. *J. Cell Biol.* **56**, 441-457.

Wright, R. L., Chojnacki, B. and Jarvik, J. W. (1983). Abnormal basal-body number, location, and orientation in a striated fiber-defective mutant of *Chlamydomonas reinhardtii*. *J. Cell Biol.* **96**, 1697-1707.

Wright, R. L., Salisbury, J. and Jarvik, J. W. (1985). A nucleus-basal body connector in *Chlamydomonas reinhardtii* that may function in basal body localization or segregation. *J. Cell Biol.* **101**, 1903-1912.